Conformational heterogeneity of the allosteric drug and metabolite (ADaM) site in AMP-activated protein kinase (AMPK)

Received for publication, May 21, 2018, and in revised form, September 5, 2018 Published, Papers in Press, September 11, 2018, DOI 10.1074/jbc.RA118.004101

Xin Gu[‡1], **Michael D. Bridges**[§1], **Yan Yan**[‡¶], **Parker W. de Waal**[‡], **X. Edward Zhou**[‡], **Kelly M. Suino-Powell**[‡], **H. Eric Xu**[‡¶], **Wayne L. Hubbell**[§], **and Karsten Melcher**[‡2]

From the [‡]*Center of Cancer and Cell Biology, Van Andel Research Institute, Grand Rapids, Michigan 49503, the* [§]*Jules Stein Eye Institute and Department of Chemistry and Biochemistry, UCLA School of Medicine, University of California, Los Angeles, California 90095-7008, and the* [¶]*VARI-SIMM Center, Center for Structure and Function of Drug Targets, The CAS Key Laboratory of Receptor Research, Shanghai Institute of Materia Medica, Chinese Academy of Sciences (CAS), Shanghai 201203, China*

Edited by Wolfgang Peti

AMP-activated protein kinase (AMPK) is a master regulator of energy homeostasis and a promising drug target for managing metabolic diseases such as type 2 diabetes. Many pharmacological AMPK activators, and possibly unidentified physiological metabolites, bind to the allosteric drug and metabolite (ADaM) site at the interface between the kinase domain (KD) in the α-subunit and the carbohydrate-binding module (CBM) in the β-subunit. Here, using double electron–electron resonance (DEER) spectroscopy, we demonstrate that the CBM–KD interaction is partially dissociated and the interface highly disordered in the absence of pharmacological ADaM site activators as inferred from a low depth of modulation and broad DEER distance distributions. ADaM site ligands such as 991, and to a lesser degree phosphorylation, stabilize the KD–CBM association and strikingly reduce conformational heterogeneity in the ADaM site. Our findings that the ADaM site, formed by the KD–CBM interaction, can be modulated by diverse ligands and by phosphorylation suggest that it may function as a hub for integrating regulatory signals.

AMP-activated kinase (AMPK)[3] is a heterotrimeric protein kinase that in mammals can form up to 12 different isoforms assembled from two alternative α-subunits (α_1 and α_2), two alternative β-subunits (β_1 and β_2), and three alternative γ-subunits (γ_1, γ_2, and γ_3) (1–3). AMPK senses the energy state of cells by competitive binding of AMP, ADP, and ATP to two exchangeable regulatory sites (CBS1 and CBS3) in its γ-subunits (4–6). In addition, AMP tightly binds to a third site (CBS4), which appears to exchange only under nonphysiological conditions (4–6). Energy stress increases the ratios of AMP and ADP to ATP, which readily changes occupancy of adenine nucleotides at the "sensor site" CBS3 to activate AMPK's kinase activity (4, 7). In turn, activated AMPK reprograms cellular metabolism, growth, and proliferation to re-establish energy homeostasis by phosphorylation of key metabolic and regulatory proteins (8–10). AMPK has also been proposed to be regulated by glycogen, which binds the carbohydrate-binding module (CBM) in the β-subunits, but this regulatory effect remains controversial (11–14).

In addition to its known physiological ligands, AMPK can be activated by the binding of pharmacological activators to the allosteric drug and metabolite (ADaM) site of AMPK (15, 16). Similar to AMP, ADaM site agonists can activate AMPK both by protection from dephosphorylation of the activation loop and by direct (phosphorylation-independent) allosteric kinase activation (16–18). In addition, AMP can also stimulate activation loop phosphorylation (19, 20). Because adenine nucleotides and their derivatives regulate many proteins in cells, they are not selective AMPK activators. In contrast, ADaM site ligands are selective for AMPK and therefore have promise as therapeutic drugs for the treatment of metabolic diseases, most prominently type 2 diabetes (10, 21, 22). A limitation of many ADaM site agonists is their relatively inefficient activation of β_2-subunit–containing AMPK isoforms, which are the predominant isoforms in human liver and skeletal muscle, two main therapeutic AMPK target organs (21, 23–25). Recent crystal structures of AMPK $\alpha_2\beta_1\gamma_1$ and $\alpha_2\beta_2\gamma_1$ bound to the α_2-biased activator SC4 have provided first insight into β_2-ADaM site-binding determinants (26).

Crystal structures of ADaM ligand-bound AMPK complexes reveal overall very similar AMPK conformations, with somewhat larger root mean square deviations in their CBMs (15, 16, 23, 26). However, several lines of evidence suggest that ADaM

This work was supported by the Jules Stein Professorship endowment (to W. L. H.), Van Andel Research Institute (to H. E. X. and K. M.), National Institutes of Health Grants R01 GM102545 and R01 GM129436 (to K. M.), R01 EY05216, T33 EY07026, and 5P41EB001980 (to W. L. H.), and R01 DK071662 (to H. E. X.), National Natural Science Foundation of China Grant 31300245 (to H. E. X.), Ministry of Science and Technology (China) Grants 2012ZX09301001 and 2012CB910403, 2013CB910600, XDB08020303, and 2013ZX09507001 (to H. E. X.), and Amway (China) (to H. E. X.). The authors declare that they have no conflicts of interest with the contents of this article. The content is solely the responsibility of the authors and does not necessarily represent the official views of the National Institutes of Health.
This article contains Table S1 and Figs. S1–S9.

[1] Both authors contributed equally to the results of this work.
[2] To whom correspondence should be addressed: Bostwick Ave. Northeast, Grand Rapids, MI 49503. Tel.: 616-234-5699; E-mail: Karsten.melcher@vai.org.

[3] The abbreviations used are: AMPK, AMP-activated kinase; CBM, carbohydrate-binding module; ADaM, allosteric drug and metabolite; DoM, depth of modulation; HDX, hydrogen deuterium exchange; MBP, maltose-binding protein; KD, kinase domain; SUMO, small ubiquitin-like modifier; Tricine, *N*-[2-hydroxy-1,1-bis(hydroxymethyl)ethyl]glycine; HO-225, 1-oxy-2,2,5,5,-tetramethylpyrrolinyl-3-methyl)-methanethiosulfonate; R734, Rigel Therapeutics 734.

sites are dynamic in solution and can adopt a number of different conformational states. First, the ADaM site ligand pocket is adaptable and its shape and size is modulated by ligand binding. For instance, we have calculated a pocket size of 486.5 Å^3 for AMPK $\alpha_2\beta_1\gamma_1$ bound to 991 (PDB 4CFE); pocket sizes of 374.5 Å^3 and 474.9 Å^3, respectively, for AMPK $\alpha_1\beta_1\gamma_1$ bound to the A769662 derivatives Cl-A769662 (PDB 4QFR) and Br_2-A769662 (PDB 4QFS); pocket sizes of 547.1 Å^3 and 522.7 Å^3, respectively, for AMPK $\alpha_1\beta_1\gamma_1$ bound to the 991 derivatives R734 and R739;[4] and pocket sizes of 195.0 and 396.1 Å^3, respectively, for apo-AMPK $\alpha_1\beta_1\gamma_1$ (PDB 4QFG) and apo-AMPK $\alpha_1\beta_2\gamma_1$ (PDB 4RER). Second, the first identified ADaM site agonist, the thienopyridone A769662, only activates β_1-subunit containing complexes, requires phosphorylation of Ser-108 of the CBM, and can synergize with AMP to fully activate AMPK even in the absence of AMPK activation loop phosphorylation (27, 28). In contrast, the cyclic benzimidazole 991 also activates β_2-containing AMPK complexes (albeit less potently than β_1-containing AMPK), does not absolutely require CBM phosphorylation for agonist activity, and in combination with AMP fails to fully overcome the requirement for activation loop phosphorylation (16, 29). Third, a 991-derivative AMPK activator, R739, selectively and robustly increases protection of the activation loop of β_2-containing AMPK against dephosphorylation without increasing direct allosteric AMPK activation.[4] Fourth, the A769662 derivative MT47-100 is an agonist of β_1-containing complexes, but an inhibitor of β_2-containing complexes (30). Fifth, the ADaM site-forming KD–CBM interaction is destabilized by glycogen, which binds the CBM distal to the ADaM site, and is stabilized by CBM phosphorylation (13), whereas adenine nucleotides constrain the CBM flexibility (4). Collectively, this indicates that ADaM site modulation through AMPK ligands is highly complex and likely proceeds through adoption of different ensembles of conformations in solution. Full understanding of AMPK regulation through ADaM site modulation therefore requires elucidation of the conformational landscapes of the ADaM site in different AMPK activity states.

To gain detailed insight into ADaM site conformational states and their differential stabilization, we site-specifically introduced pairs of nitroxide spin labels into AMPK to determine the distributions of distances between their electron spins by DEER spectroscopy. In contrast to continuous wave electron paramagnetic resonance (EPR) methods, which measure short distances between spin pairs (5–25 Å) via spectral line broadening, DEER provides interspin distance distributions in the 18–80-Å range with high accuracy by analysis of an acquired dipolar evolution trace (31–33). This dipolar evolution function is analyzed to yield interspin distance information by way of background signal subtraction and Pake transform. The extent to which the position and width of peaks in a DEER distance distribution are reliably determined depends, among other things, on the data collection time (32), where the most reliable fits are those where at least one full dipolar oscillation is visible in, and thus fittable from, the trace. Regarding the data presented under "Results": for distances between 20 and 45 Å both the position and width of DEER peaks are reliable (the boundary of which is indicated by a red mark on the *x*-axis of distance distribution plots, see, *e.g.* Fig. 2*A*); between 45 and 60 Å, the position, but not the width of peaks is reliable (this region is bounded by a green mark on the *x*-axis), whereas at distances greater than 60 Å, the presence of interacting spin populations are indicated, but neither their position nor width is reliable. Because different protein preparations have variations in activity and labeling efficiency, Fig. S1 visualizes the level of spectral reproducibility from two pairs of independent protein preparations.

The amplitude of the dipolar evolution function, the "depth of modulation" (DoM), can be used to estimate the fraction of spins involved in discrete pairwise interactions within the distance range of the method (32), thus providing a means to detect partial dissociation of a region bearing the labels. For example, if a domain bearing one label partially dissociates from the rest of the protein, thus moving the interspin distance outside of the detectable DEER range (≥80 Å), the DoM will decrease in proportion to the fraction dissociated. Although other biophysical techniques such as FRET or hydrogen deuterium exchange (HDX) provide insight on averaged conformational states, DEER identifies distinct conformational states and their fractional occupancies. Using this experimental approach, we demonstrate that the ADaM site is only partially formed and highly heterogeneous in the apo-state, induced and greatly stabilized by ADaM site agonists, and modulated by phosphorylation.

Results

A cysteine-free version of AMPK is catalytically active and regulated by adenine nucleotides and 991

To site-specifically introduce DEER spin labels into the AMPK holo-complex, we first mutated the 13 exposed cysteines in AMPK (Table S1). This allowed us to chemically introduce nitroxide spin labels either into endogenous, exposed cysteines that we selectively excluded from mutation or into cysteines introduced at selected positions by site-directed mutagenesis. Given the pharmacological interest in the ADaM site of β_2-containing AMPK (21), we selected the $\alpha_1(11–550)$–$\beta_2(76–272)$–$\gamma_1(24–327)$ complex, at the time the only β_2-containing holo-AMPK complex of known structure (PDB 4RER) (13), for this study. We further introduced a maltose-binding protein (MBP) tag at the N terminus of the α_1-subunit, which we have found to increase stability and solubility of the complex. This "Cys-free" AMPK assembles normally and stochiometrically and is, as WT AMPK, phosphorylated by the AMPK upstream kinase CaMKKβ at its α- and β-subunits (Figs. S2*A* and S3, *A* and *B*). It has been reported that AMPK with α_2 C130A and C174A mutations cannot be activated by energy stress in cells or *in vitro* (34). However, Cys-free MBP-$\alpha_1\beta_2\gamma_1$ AMPK, in which the corresponding α_1 residues Cys-132 and Cys-176 are mutated to Ala and Ser, respectively, is clearly activated by AMP (although it has reduced catalytic activity). This protein is also activated by the ADaM site ligand 991, and not by

[4] Y. Yan, X. E. Zhou, H. E. Xu, and K. Melcher, unpublished data.

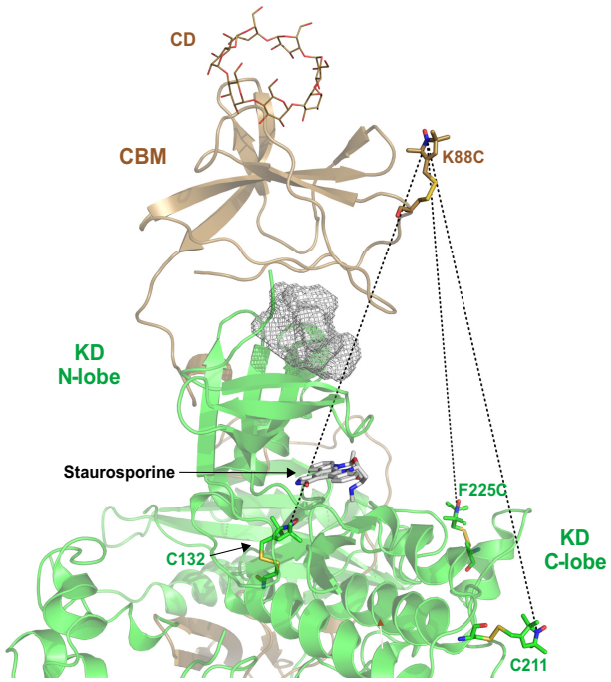

Figure 1. Visualization of the three interaction pairs in AMPK $\alpha_1\beta_2\gamma_1$ (PDB code 4RER) selected for DEER analysis. Nitroxide spin label orientations were determined by unbiased energy minimization. *Gray mesh*, empty ADaM site ligand-binding pocket; *CD*, cyclodextrin.

the β_1-specific A769662 (Fig. S2*B*), a very similar behavior to that of WT AMPK (16, 27, 35).

The catalytic center of protein kinases is located in a substrate-binding cleft between the kinase N- and C-lobes. The two lobes are connected by a flexible hinge that allows the two lobes to move relative to each other to adopt two alternative ensembles of conformations: open conformations in the absence of bound substrate and closed conformations, indicative of substrate-bound, active kinases (36). In this study, we focused on the interspin distances between one nitroxide spin label introduced into a solvent-exposed site (K88C) in the CBM and a second introduced into one of three distinct sites of the kinase domain (KD) C-lobe (Cys-132, Cys-211, and F225C; Fig. 1, and Figs. S3*C*, S4, and S5). The high affinity nonhydrolyzable ATP-competitive inhibitor staurosporine arrests kinase domains in a near closed state (37). Crystal structures suggest that ADaM site ligands modulate both the CBM–KD interface (through simultaneous binding of both the CBM and KD) as well as the KD conformation (open/closed equilibrium through induction of a helix in the CBM linker that stabilizes the αC helix of the KD in its active conformation) (15, 16). Thus distances between a spin label in the CBM domain and one in the C-lobe of the KD allowed us to probe the effects of ligands on only the ADaM site in the presence of staurosporine and on both the ADaM site and kinase domain in the absence of staurosporine.

We purified Cys-free AMPK with three combinations of (re)introduced cysteines: (i) β_2K88C–α_1C132; (ii) β_2K88C–α_1C211; and (iii) β_2K88C–α_1F225C. The spatial vector that connects β_2K88C (corresponds to human β_1K89) and α_1C132 (corresponds to human α_2C130) passes through or borders both the ADaM site, as indicated by the position of 991 in the corresponding structure of 991-bound *p*-AMPK $\alpha_2\beta_1\gamma_1$ + AMP + staurosporine (PDB 4CFE, Fig. S5) (16), and the KD catalytic cleft, as indicated by the position of staurosporine ("proximal interaction"). In contrast, the longer spatial vectors between the other two pairs of residues are more distant to both ADaM site and KD cleft ("distal interactions"). As negative controls, we purified Cys-free AMPK preparations with only a single (re)introduced cysteine (only β_2K88C, only α_1C132, only α_1C211, and only α_2F225C). As positive control, we left both α_1C132 and α_1C211 nonmutated. These two cysteines both reside within the conformationally stable kinase C-lobe. We phosphorylated part of each AMPK preparation with CaMKKβ, re-purified the proteins, chemically introduced sulfhydryl-specific nitroxide spin labels, and removed excess labeling reagents. Finally, we confirmed activity and regulation of the singly and dually labeled preparations prior to DEER spectroscopy. As expected, the four singly labeled control preparations yielded DEER signals indistinguishable from background, whereas the α_1C132 + α_1C211 positive control yielded a sharp single 31-Å peak (Fig. 2*A*), close to the 31.8-Å distance between the spin labels modeled into the 4RER structure by Rosetta energy minimization (see "Experimental procedures").

The apo-ADaM site exhibits a high degree of structural heterogeneity

In striking contrast to the above single intra-C-lobe distance distribution in solution, all spectra of CBM–KD spin label pairs in AMPK not bound to an ADaM ligand showed broad distance distributions with multiple peaks (Fig. 2, *B–D*). The gray shading represents the extent of variation in the distance distribution allowed by the data, and hence represents an uncertainty in the distribution. As is evident, the uncertainty is much larger here than in the case of Fig. 2*A*. Thus, in the absence of ADaM site ligands, the CBM–KD complex can adopt several conformational states, both for nonphosphorylated (Fig. 2*B*), phosphorylated (*p*-; Fig. 2*C*), and staurosporine-stabilized, phosphorylated AMPK (Fig. 2*D*).

Pharmacological ADaM site ligands conformationally constrain the ADaM site

When we added the ADaM site ligand 991, or its derivatives R734 and R739 (all 10 μM, each), to nonphosphorylated AMPK, all three compounds dramatically constrained the proximal β_2K88C–α_1C132 interaction to a predominant distance of 40 Å for 991, R734, and R739 with strongly depopulated long distance peaks (*left column*, Fig. 3). Even though β_2K88 is located in a loop in both the AMPK $\alpha_1\beta_2\gamma_1$ apo and $\alpha_2\beta_1\gamma_1$/991 structures, the distinct single distance peaks indicate that these compounds largely fix the relative position of Lys-88. For the distal β_2K88C–α_1C211 and β_2K88C–α_1F225C interactions (Fig. 3, *middle* and *right columns*, respectively), 991 and derivatives largely depopulated the dominant DEER distance peak at ~41 Å and in the case of β_2K88C–α_1C211, 991, and R734 shifted the ~57 Å peak by 3–5 Å to a shorter distance. Therefore, these ligands strongly reduce ADaM site heterogeneity, presumably by stabilizing the CBM–KD interaction through their direct interaction with both CBM and KD (15, 16). In addition, ADaM site ligand binding induces a small expansion of the site (indi-

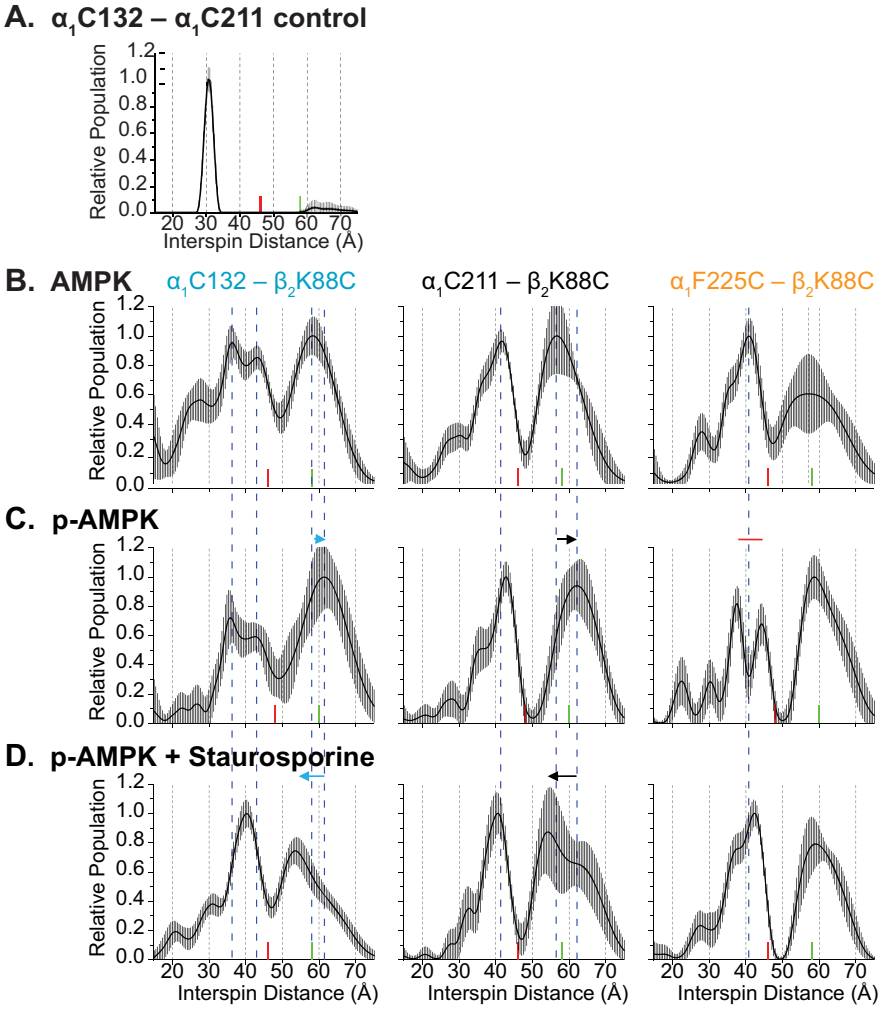

Figure 2. The ADaM site adopts multiple conformations in apo-state. *A*, control DEER measurement. *B–D*, DEER spectra of AMPK in nonphosphorylated (*B*), phosphorylated (*p*-) (*C*), and phosphorylated and staurosporine-bound state (*D*). The *gray shading* indicates the uncertainty range; the *red* and *green vertical bars* on the *x*-axis indicate the confidence borders for peak width and position, respectively. Data in *C* and *D* are from the same protein preparation (phosphorylated AMPK) in the presence or absence of staurosporine.

cated by *arrows* in Fig. 3). Although all AMPK structures in complex with ADaM ligands were solved in the context of phosphorylated (or with phosphomimetic mutations) AMPK bound to staurosporine and AMP, we note that all show a compound-induced extension of the ADaM site pocket (see Introduction). In the only set of crystal structures of the same AMPK protein, *p*-AMPK $\alpha_1\beta_1\gamma_1$ + AMP + staurosporine, in the presence and absence of an ADaM agonist, the agonist Cl-A769662 had no effect on the distance of the corresponding β_1K89–α1C209 interaction and slightly increased the distances of the other two DEER interactions pairs (15).

KD and CBM are partially dissociated in the absence of ADaM site ligands

In nonphosphorylated apo-AMPK, the distal α_1C211–β_2K88C and α_1F225C–β_2K88C interactions exhibited low DoM (Figs. S7–S9). Upon incubation with the ADaM site ligands, particularly 991 and R739, the DoM of these same labeled protein preparations increased appreciably (3-fold in the presence of 991; Figs. S7–S9), indicating that spin label distances in a substantial fraction of apo-AMPK are outside of the detectable DEER range (≥80 Å), but brought into range by ligand binding. In contrast to the two distal interactions, the DoM of the α_1C132–β_2K88C interaction reproducibly increased only weakly upon addition of 991, likely reflecting the distance constraints of this interactions imposed by the CBM linker (see "Discussion" and summary cartoon in Fig. 9). Although a structure of nonphosphorylated, apo-AMPK with resolved CBM is unavailable, these data are consistent with luminescence proximity and structure results that indicate partial CBM dissociation (13).

We further validated the ability of these compounds to restrict partial CBM dissociation of a *trans* interaction between the isolated KD and CBM using an AlphaScreen luminescence proximity assay (Fig. 4*A*). This assay is sensitive both to the distance of the two interacting domains (the shorter the distance, the stronger the signal) as well as to the fraction of CBM and KD that interact with each other (the higher the fraction, the stronger the signal). As shown in Fig. 4*B* and Fig. S6, 991 and to a lesser degree its less potent derivatives R734 and R739

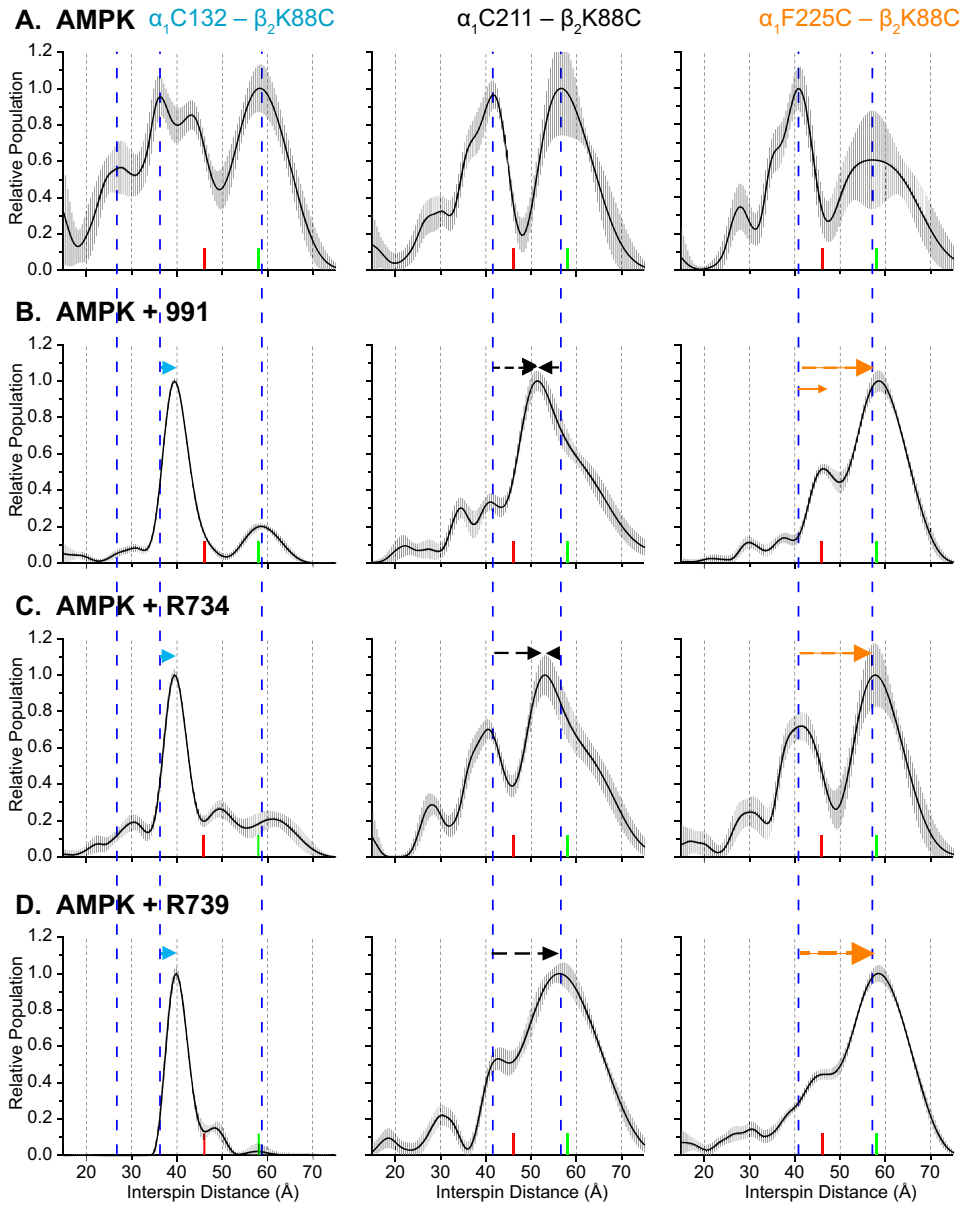

Figure 3. 991 and 991 derivatives conformationally stabilize the ADaM site. *A–D*, DEER spectra of nonphosphorylated AMPK in apo-state (*A*; same as Fig. 2*B*), or bound to 991 (*B*), R734 (*C*), or R739 (*D*). All data are from the same protein preparations in the presence or absence of the indicated ligands.

increased the luminescence signal, even though the distance between CBM and KD within the DEER detection range increases. This indicates that these compounds indeed decrease dissociation between the KD and CBM. Interestingly, 991 dose dependently increased the interaction between the KD and the β_2–CBM at least as much as the interaction with the β_1–CBM, suggesting that preferential activation of β_1 complexes by 991 is likely not only due to forming more stable complexes.

Phosphorylation alters short and long distance KD–CBM interactions

Phosphorylation of CBM Ser-108 is thought to stabilize the ADaM site-forming KD–CBM interaction through a charge interaction of the CBM phosphate group with a lysine side chain in the KD (13, 15, 16). In agreement, addition of 991 to phosphorylated AMPK increased the DoM ≤2-fold, consistent with a smaller fraction of KD–CBM dissociation in phosphorylated *versus* nonphosphorylated apo-AMPK (Figs. S7–S9). In addition, within the range of the DEER technique, phosphorylation shifted the far 55–60 Å peaks of the α_1C132–β_2K88C and α_1C211-β_2K88C interactions to larger distances (just beyond the 60 Å reliability mark), whereas the proximal peaks in the 25–30-Å range depopulated (compare Fig. 5, *B* and *C*).

Phosphorylation of 991-bound AMPK had little effect on the dominant β_2K88C–α_1C132 and β_2K88C–α_1C211 peaks, but shifted the β_2K88C–α_1F225C peaks to shorter distances (compare Fig. 5, *B* and *C*). Moreover, whereas it is difficult to compare the DoM of different protein preparations (phosphorylated *versus* nonphosphorylated AMPK), we note that phosphorylation of 991-bound AMPK had no noticeable effect

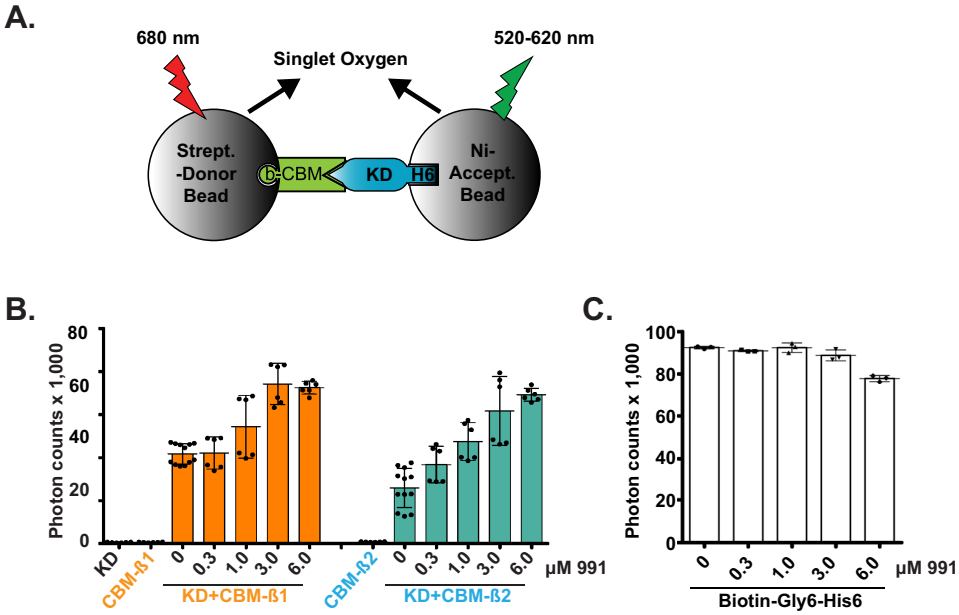

Figure 4. 991 stabilizes the KD–CBM interaction. *A,* cartoon of the AlphaScreen experiment. Nonphosphorylated, biotinylated CBM, and His_6-tagged KD were immobilized on streptavidin-coated donor beads and nickel-acceptor beads, respectively. Donor beads contain a photosensitizer that upon activation at 680 nm converts ambient oxygen into short-lived singlet oxygen. If acceptor and donor beads are brought into close proximity by CBM–KD interaction, energy is transferred from singlet oxygen to thioxene derivatives in the acceptor beads resulting in emission of light at 520–620 nm. *B,* interaction between KD and CBM in the absence and presence of increasing concentrations of 991. Incubation of donor and acceptor beads with only KD or only CBM serve as controls. *C,* high concentrations (6 μM) of 991 nonspecifically reduce the AlphaScreen signal by about 20%. Increasing concentrations of 991 were incubated with donor and acceptor beads and a biotin-Gly^6-His_6 peptide, which constitutively brings donor and acceptor beads into proximity. Note that due to the small nonspecific inhibition, stabilization of the CBM–KD interaction by 6 μM 991 is underestimated. $n = 6$ (2 biological replicates of 3 technical replicates, each, for CBM–KD interaction, $n = 3$ (3 technical replicates) for biotin-Gly_6-His_6 control); *error bars* = S.D.

on the exhibited DoM value, suggesting that 991 at a concentration of 10 μM may efficiently stabilize the KD–CBM interaction independent of the phosphorylation state of AMPK.

Staurosporine constrains the AMPK catalytic cleft differently than 991

Addition of staurosporine to phosphorylated apo-AMPK induced clear changes in DEER distance distributions (Fig. 2*D*) with small reductions in the DoM (Figs. S7–S9). Specifically, positions of the longest distance peaks observed for β_2K88C–α_1C132 and β_2K88C–α_1C211 decreased by 5–10 Å, whereas the peaks centered around ~40 Å narrowed, indicating a reduction in structural heterogeneity (Fig. 2*D*). These changes likely reflect the stabilization of the near closed KD conformation that has been observed in KD crystal structures (37). Unexpectedly, when we added staurosporine to 991-complexed AMPK, structural heterogeneity of the proximal (β_2K88C–α_1C132) interaction increased (Fig. 5*D*), whereas distances of the distal interaction shifted by 3–5 Å, strongly indicating that 991 and staurosporine stabilize distinct sets of KD conformations (see "Discussion"). Note that the experimentally determined DEER distances in the contexts of both *p*-AMPK $\alpha_1\beta_2\gamma_1$/991 (β_2K88C–α_1C132: 40 Å, β_2K88C–α_1C211: 52 Å, β_2K88C–α_1C225: 40 Å) and -$\alpha_1\beta_2\gamma_1$/991 + staurosporine (β_2K88C–α_1C132: 43 Å, β_2K88C-α_1C211: 47 Å, β_2K88C–α_1C225: 43 Å) are similar to the distances between the spin labels modeled into the structure of *p*-AMPK $\alpha_2\beta_1\gamma_1$/991 + staurosporine + AMP (PDB 4CFE; β_1K89C–α_2C130: 41 Å, β_1K89C–α_2C209: 52 Å, β_1K89C–α_2C223: 47 Å).

AMP and ATP impart slight interspin distance changes in phosphorylated AMPK

AMP and ATP competitively bind the CBS sites in the AMPK γ-subunit. HDX-MS has demonstrated that ATP, and more strongly AMP, conformationally stabilize the CBM, suggesting conformational connectivity between the CBS sites in the γ-subunit and the CBM of the β-subunit (4). In addition, ATP, staurosporine, and at high concentrations also AMP (19) bind the ATP-binding site in the catalytic cleft of the KD. AMP and ATP (200 μM, each) binding to nonphosphorylated AMPK had relatively minor effects on DEER distance distributions (Fig. 6), whereas binding to phosphorylated AMPK induced slightly more noticeable changes (Fig. 7). In particular, the far distance (~62 Å) β_2K88C–α_1C211 peak seems to broaden to two separate peaks, similar as in the presence of staurosporine (Fig. 2*D*), whereas the β_2K88C–α_1F225C ~38 Å peak upon ATP or staurosporine binding became less populated and the 44-Å peak slightly shifted and more populated (Fig. 7, *B–D*). Together, this suggests that AMP and ATP may mildly affect KD–CBM conformational states, partially through binding to the catalytic cleft.

Glycogen destabilizes the interaction between KD and CBM in trans, but does not induce unambiguous changes in ADaM site DEER spectra in the context of holo-AMPK

The interaction between the AMPK KD and CBM can be reconstituted in *trans* using isolated domains (13). Glycogen binding destabilizes the *trans* CBM–KD interaction and increases the CBM–KD distance in the context of holo-AMPK,

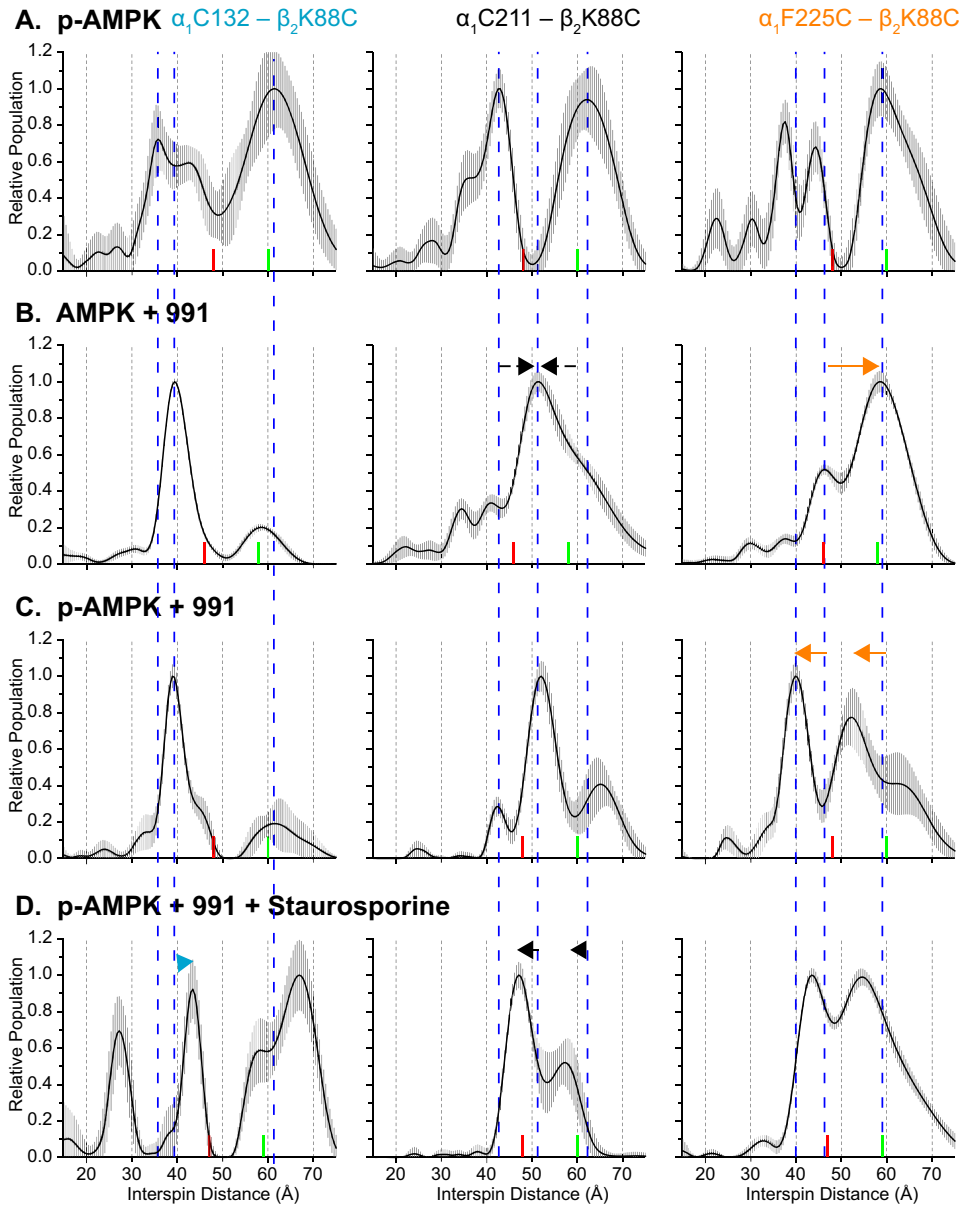

Figure 5. Phosphorylation and staurosporine modulate the 991-occupied ADaM site. *A–D,* DEER spectra of phosphorylated AMPK in apo-state (*A*; same as Fig. 2*C*), nonphosphorylated AMPK bound to 991 (*B*; same as Fig. 3*B*), phosphorylated AMPK bound to 991 (*C*), and phosphorylated AMPK bound to 991 and staurosporine (*D*). All data in *A*, *C*, and *D* (phosphorylated AMPK) are from the same protein preparations in the presence or absence of the indicated ligands.

most prominently for nonphosphorylated AMPK (13). Fig. 8*A* recapitulates the *trans* interaction data as full dose-response curves for both WT AMPK $\alpha_1\beta_2\gamma_1$ and AMPK $\alpha_1\beta_2\gamma_1$ W99G, a loss-of-function mutation in the carbohydrate-binding loop of the CBM (14, 38). The compromised ability of glycogen to dissociate the *trans* KD–CBM interaction in the W99G mutant (4 orders of magnitude increased IC_{50}) strongly implies that the effect of glycogen on the interaction between the isolated KD and CBM depends on the direct binding of glycogen to the carbohydrate-binding loop. Note that whereas cellular glycogen concentrations are always above the IC_{50} determined in Fig. 8*A*, in cells glycogen binding requires dephosphorylation of the CBM carbohydrate-binding loop (39).

When we recorded DEER spectra of the same preparations of nonphosphorylated AMPK in the absence and presence of 2 mg/ml of glycogen, we observed small changes in DEER spectra (the 36- and 43-Å β_2K88C–α_1C132 peaks collapsed to a single 39-Å peak and the 57-Å β_2K88C–α_1C211 shifted to 54 Å; Fig. 8). These changes are comparable with changes that can be observed with different, independent preparations of the same AMPK protein (see Fig. S1*B*). In the absence of additional experiments, we can therefore not conclude that glycogen induces changes in the DEER distance distributions analyzed.

Discussion

AMPK activation reduces blood glucose levels, improves insulin sensitivity, inhibits fat synthesis and proliferation, and mediates many of the beneficial effects of exercise and weight loss. AMPK is therefore an attractive target for the treatment of metabolic diseases. The most promising site to therapeutically target AMPK is the ADaM site. Recently, Pfizer and Merck have both developed first specific ADaM site-targeting AMPK ago-

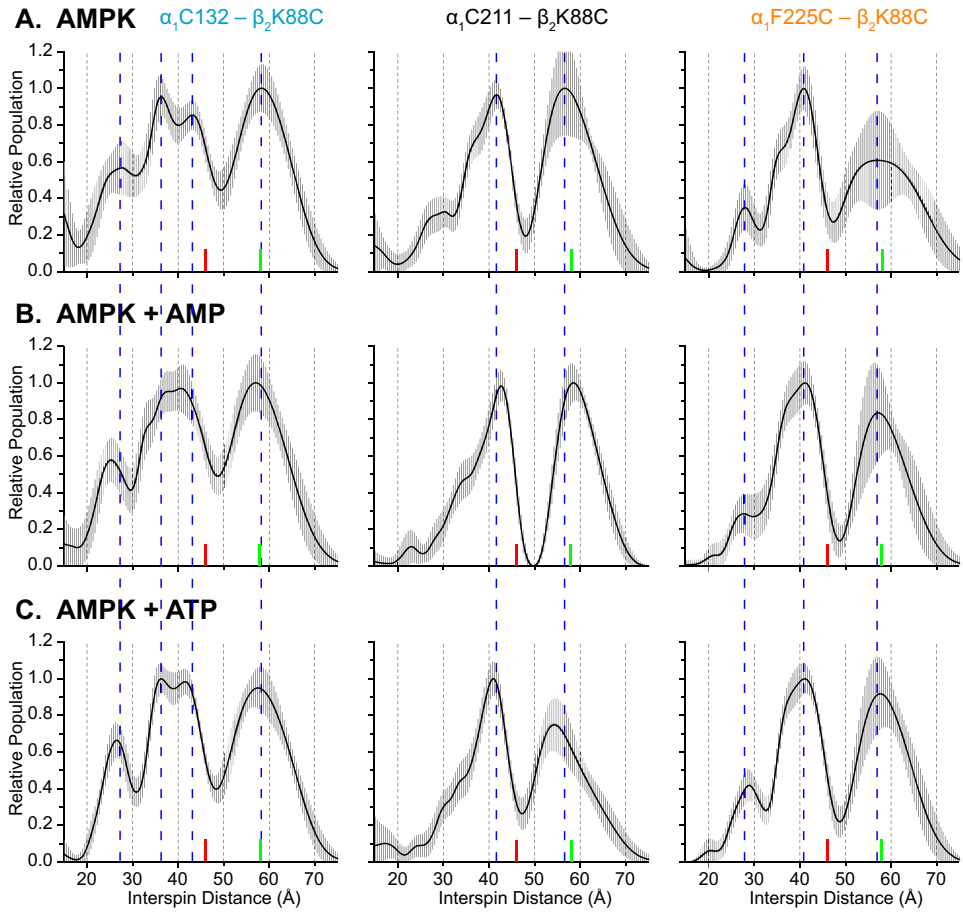

Figure 6. AMP and ATP do not strongly modulate CBM/KD C-lobe distances in nonphosphorylated AMPK. *A–C,* DEER spectra of nonphosphorylated AMPK in apo-state (*A*; same as Fig. 2*B*), and bound to AMP (*B*), and ATP (*C*). All data are from the same protein preparations in the presence or absence of the indicated ligands.

nists that can efficiently activate the therapeutically important β_2-containing AMPK complexes *in vivo* (23, 24). Given the high potential of the ADaM site for the design of AMPK-activating therapeutics, as well as its potential as binding pocket for hypothesized, novel physiological AMPK regulators, it is important to understand its conformational landscape and dynamics. Currently, only one crystal structure of an ADaM site ligand bound to a β_2-containing AMPK complex has been determined (26), which represents a single conformation snapshot. In contrast, biochemical characterization suggests that different ligands and different β subunits induce different AMPK activity states. DEER spectroscopy is a powerful biophysical tool to study the structural heterogeneity and conformational landscape of dynamic proteins by determining the distributions of interspin distances between site-specifically introduced spin labels under various conditions inaccessible to other techniques such as NMR, FRET/FCS, and X-ray crystallography. Moreover, observed changes in the DEER modulation depth when comparing samples in different ligand or phosphorylation conditions can provide information on the presence of spin label pairs beyond a distance of 80 Å, which may be indicative of full or partial protein domain dissociation with all other experimental conditions held constant. A limitation in DEER accuracy is that the introduction of mutations and spin labels in only partially solvent accessible local environments may induce local structural distortions and introduce a systematic deviation in the distance measured from the native physiological distance. Importantly, these errors should not preclude identification of relative distance changes in the same labeled protein under two different conditions.

Two crystal structures of phosphorylated, AMP- and staurosporine-bound apo-AMPK have visualized the CBM bound to the KD, similar as in AMPK bound to ADaM site ligands, although with some CBM structural heterogeneity (13, 15). In contrast, in a low resolution structure of nonphosphorylated apo-AMPK the CBM was not resolved and the CBM linker was displaced (13). In addition, as first pointed out by Calabrese *et al.* (15), Ser-108 of the CBM can be phosphorylated through cis-autophosphorylation (*i.e.* by the KD of the same AMPK heterotrimer) (28), which would require partial dissociation of the CBM–KD packing seen in the crystal structures to allow nonphosphorylated Ser-108 access to the KD catalytic cleft. Our DEER data demonstrate that the CBM can indeed partially dissociate in solution in apo-AMPK as evidenced by the low DoM of the two distal interactions and the strong DoM increase upon addition of ADaM site ligands. We have further shown by an AlphaScreen luminescence proximity assay that 991, and with less certainty also R734 and R739, can directly stabilize the interaction between isolated CBM and KD proteins. Importantly, when the CBM–KD interaction is dissociated in the context of holo-AMPK, CBM and KD still remain in proximity as they remain part of the same heterotrimeric AMPK complex.

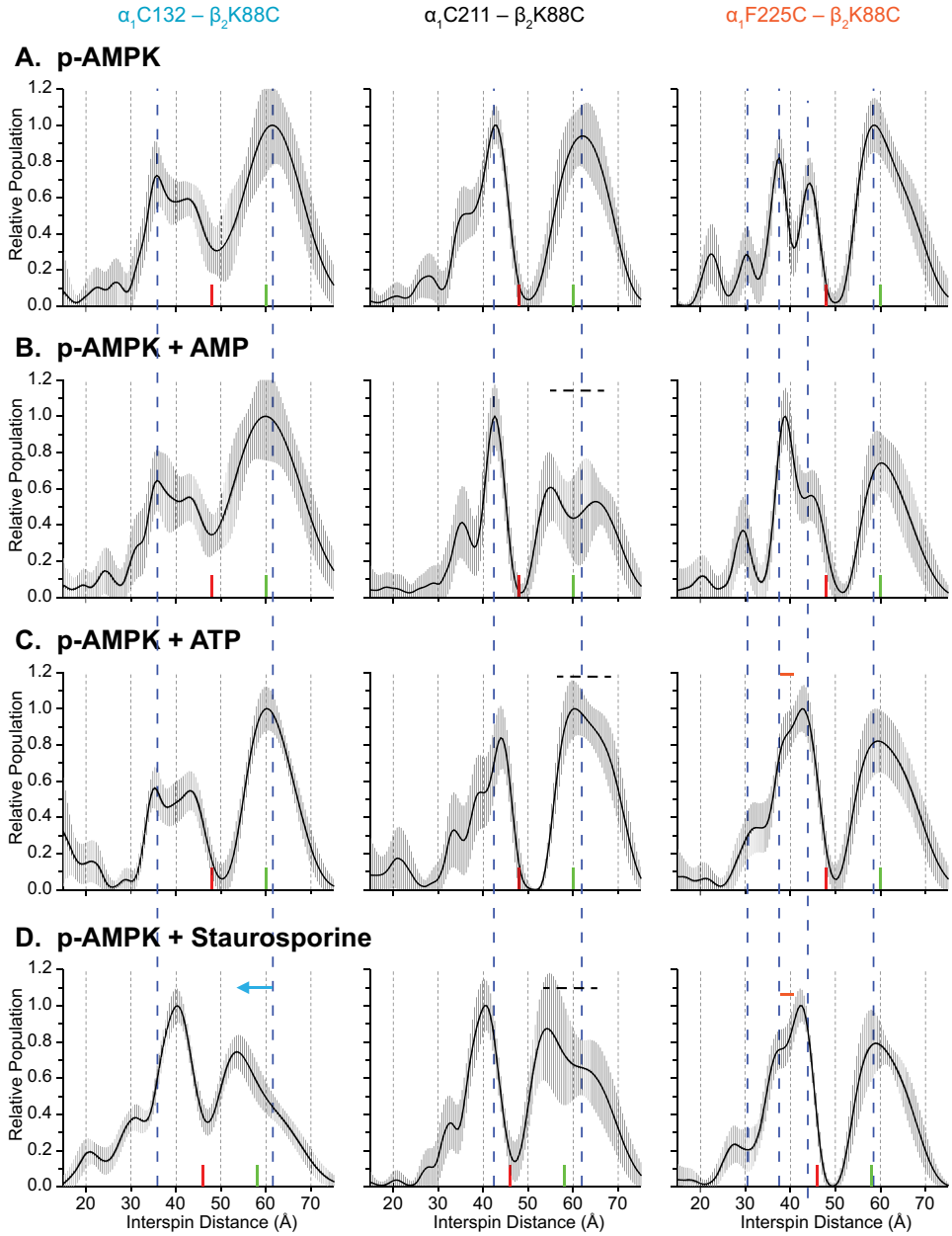

Figure 7. AMP, ATP, and staurosporine stabilize the KD in different states. *A–D,* DEER spectra of phosphorylated AMPK in apo-state (*A*), and bound to AMP (*B*), ATP (*C*), or staurosporine (Sto) (*D*). Data in *A–C* are from the same protein preparations, whereas data in *D* are from a different protein preparation.

Position of the CBM is mainly constrained by the CBM linker, which at least in active AMPK makes intensive interactions with the activation loop of the KD (7, 13, 16). These constraints are the likely reason that the shorter proximal interaction, which is closer to the linker, remains largely within a range of <70 Å. Within the range of the technique, the data visualize the high conformational heterogeneity of the CBM–KD interface with a broad range of distance distributions. The ADaM agonists 991, R734, and R739 dramatically constrained the broad distributions, especially for the proximal interaction. Together, this indicates that binding of ADaM site ligands both counter CBM dissociation and conformationally stabilize the CBM–KD interaction (Fig. 9).

In addition to ADaM site ligands, both phosphorylation and staurosporine binding modulate the analyzed interactions as expected from structural and biochemical analysis. In apo-AMPK, the phosphate group of CBM pSer-108 stabilizes the CBM–KD interaction by charge interaction with the KD (13, 15). In 991- and A769662-bound AMPK, the phosphate group directly binds and stabilizes the ligand, consistent with a robust increase in ligand affinity upon Ser-108 phosphorylation (15, 16, 27). Although staurosporine was expected to conformationally constrain the analyzed interactions by stabilization of a near-closed KD conformation, in the presence of 991 it increased structural heterogeneity and shifted the dominant DEER distance peaks. Staurosporine stabilizes kinase domains by high affinity binding to their dynamic catalytic clefts, whereas ADaM site ligands do so by inducing formation of a helix in the CBM linker ("C-interacting helix") that packs against the KD αC helix (15, 16), a key regulatory element to

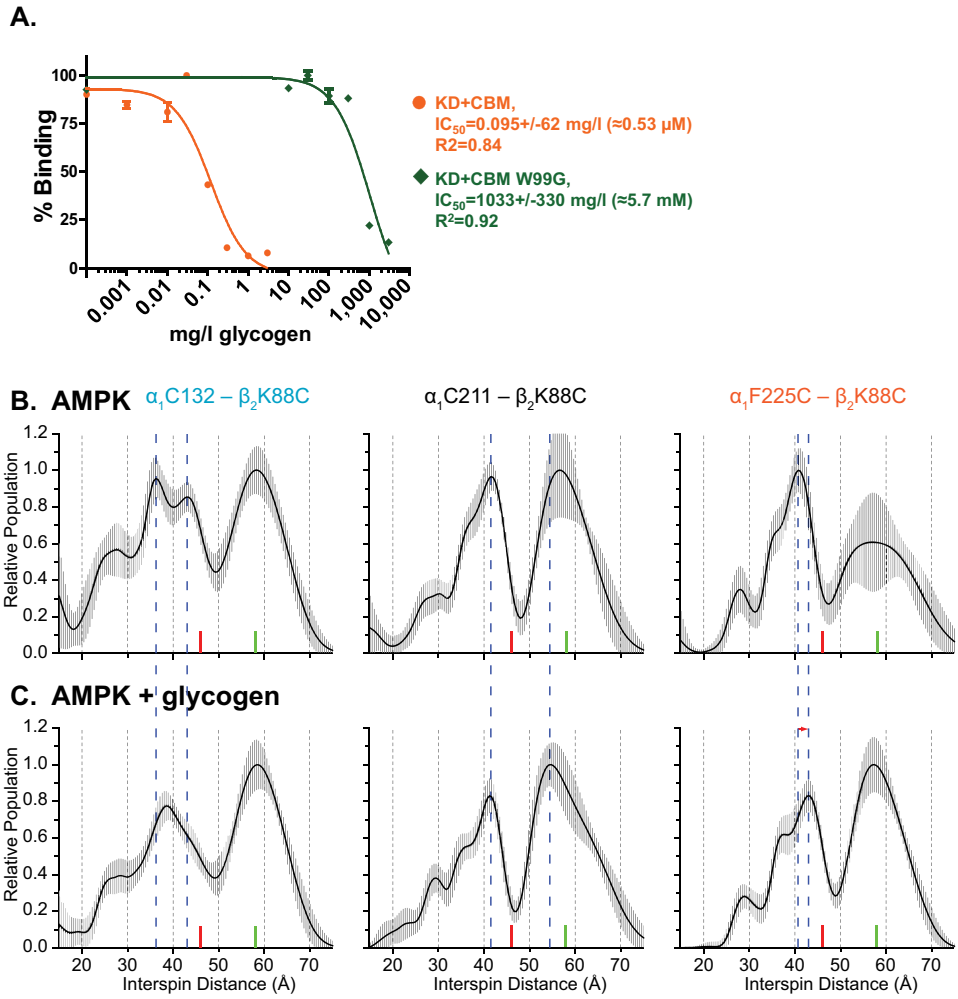

Figure 8. Glycogen does not strongly modulate the ADaM site distance distributions in non-phosphorylated AMPK. *A,* glycogen dissociates a trans interaction between KD and CBM. *B* and *C,* DEER spectra of non-phosphorylated AMPK in the apo-state (*B*; same as Fig. 2*B*), and bound to glycogen (*C*). Data in *B* and *C* are from the same protein preparation that only differed by the absence or presence of glycogen.

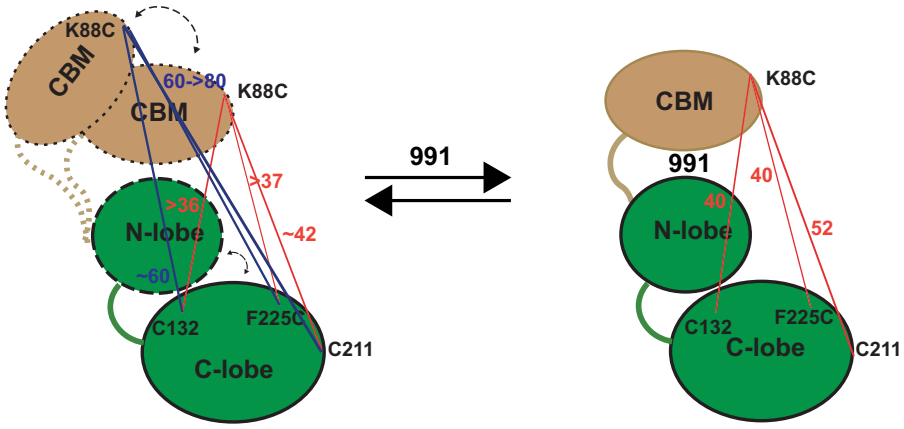

Figure 9. Cartoon illustration and model of 991-induced conformational changes in *p*-AMPK. The presence of 991 induces single predominant DEER peaks with high DoM and distances as predicted based on the crystal structure of 991-bound *p*-AMPK (4CFE). In the absence of ADaM ligands, the DEER spectra exhibit broad distance distributions with two distance clusters (*red* and *blue*) and partial CBM dissociation from the ADaM site, indicated by the low DoM of the β_2K88C–α_1C211 and β_2K88C–α_1F225C spectra. The comparatively high DoM of the proximal β_2K88–α_1C132 interaction likely reflects its distance constraint by the CBM linker. Note that distances in the presence of 991 are slightly longer than those of the most dominant peaks in the short distance cluster in the absence of 991, indicating a 991 binding-induced small extension of the ADaM site. The approximate positions of the spin-labeled residues β_2K88, α_1C132, α_1C211, and α_1F225 is based on the crystal structure of 991-bound *p*-AMPK $\alpha_2\beta_1\gamma_1$ (4CFE). *Solid red* and *cyan lines* represent dominant DEER distances (numbers indicate distances in Å). The distance listed for each cluster only shows the most populated distance peak. *Dashed outlines* of the CBM, KD N-lobe, and CBM linker indicate their dynamic conformations in the absence of 991.

shift the catalytic cleft equilibrium to the closed conformation (36, 40). Although all structures of holo-AMPK have been determined in the presence of staurosporine, comparison of structures in which the CBM linker adopts the C-interacting helix (*e.g.* PDB 4CFE, 4CFF, 4QFR, 4QFG, and 4QFS) with the sole structure in which the C-interacting helix is not induced (4RER) indeed indicates a small shift of the KD N-lobe toward the C-interacting helix and away from the KD C-lobe. These data therefore suggest that ADaM site ligands stabilize formation of an active KD conformation that is slightly different from that stabilized by staurosporine (and possibly AMP), and that therefore the presence of both staurosporine and 991 induces formation of a broader distance distribution than that of 991 in the absence of staurosporine. In contrast to AMPK phosphorylation and staurosporine binding, adenine nucleotides, which reduce hydrogen/deuterium exchange in the CBM (4), and glycogen, which destabilizes the interaction between the isolated CBM and kinase domains, induce only subtle changes in the DEER spectra of analyzed interactions.

In conclusion, the ADaM site, formed by CBM–KD interaction, is the key regulatory site for therapeutic AMPK intervention. Although the CBM–KD interaction is partially dissociated and highly heterogeneous in the apo-state, ADaM site ligands dramatically stabilize the association and reduce ADaM site heterogeneity. Phosphorylation, staurosporine, and possibly adenine nucleotides and glycogen further modulate the CBM–KD interaction, suggesting that the ADaM site may be a hub for integrating regulatory signals.

Experimental procedures

Generation of Cys-free AMPK

To introduce Cys mutations into the α_1 subunit, a codon-optimized α_1 subunit with 8 mutations (C108S, C176S, C229R, C299S, C304S, C312S, C416Y, and C494P) was synthesized by GenScript Biotech (Piscataway, NJ). Cys mutations in the β_2- and γ_1-subunits (β_2-C178A and γ_1-C131S) were introduced by site-specific mutagenesis using the QuikChange method (Agilent Technologies, Santa Clara, CA). α_1-C132A and α_1-C211S were introduced by site-specific mutagenesis where required. All mutations were verified by DNA sequencing. Mutant open reading frames were cloned into a tri-cistronic *Escherichia coli* expression plasmid as described (13), only that the His_6 tag was replaced with a codon-optimized MBP tag.

Spin labeling

Phosphorylated or nonphosphorylated AMPK protein was concentrated to about 10 mg/ml in 50 mM MES, pH 6.8, 150 mM NaCl, 5 mM $MgCl_2$, 0.5 mM EDTA, and 10% glycerol, mixed at a 1:10 molar ratio with 1-oxy-2,2,5,5,-tetramethylpyrrolinyl-3-methyl)-methanethiosulfonate (HO-225, Toronto Research Chemicals Inc., Toronto, Canada) and incubated at 4 °C overnight. Excess HO-225 was removed by desalting through a GE Healthcare PD-10 column, and glycerol was added to a final concentration of 20%. Test compounds were added to final concentrations of 200 μM for AMP and ATP; 10 μM for 991, R734, and R739; and 2 mg/ml for glycogen. Test compounds were incubated with labeled proteins for 30 min on ice prior to freezing in liquid nitrogen. Final AMPK concentrations were between 50 and 100 μM.

AMPK expression and purification

AMPK expression plasmids were transformed into *E. coli* BL21(DE3). Cells were grown in LB medium to an A_{600} of ~1 at 28 °C and induced with 100 μM isopropyl β-D-thiogalactopyranoside at 16 °C overnight. Cell pellets were re-suspended in 25 mM Tris, pH 8.0, 300 mM NaCl, 10% (v/v) glycerol, 5 mM $MgCl_2$, 1 mM EDTA, 2 mM DTT, and lysed by French Press with pressure set to 900 Pa. Lysates were cleared by centrifugation for 50 min at 20,000 × *g*, passed over a 10-ml MBP Trap HP column (GE Healthcare, Little Chalfont, UK), and eluted with 25 mM Tris, pH 8.0, 300 mM NaCl, 10% (v/v) glycerol, 5 mM $MgCl_2$, 1 mM EDTA, 2 mM DTT, and 20 mM maltose. Phosphorylated AMPK was generated by incubation with a 0.02-fold molar ratio of CaMKKβ in 0.2 mM AMP, 0.2 mM ATP, 2 mM $CaCl_2$, 10 mM DTT, and 1 μM calmodulin at room temperature overnight (16 h). The phosphorylated AMPK was re-purified by size-exclusion chromatography through a HiLoad 26/60 Superdex 200 column (GE Healthcare) in 50 mM MES, pH 6.8, 150 mM NaCl, 5 mM $MgCl_2$, 0.5 mM EDTA, and 10% (v/v) glycerol. The protein eluted from the gel filtration column at a volume corresponding to the size of a monomeric complex at a purity ≥95% as judged by SDS-PAGE.

His_6-GST-KD (human AMPK α1, residues 11–281) was expressed from pET24 (Novagen) and induced and lysed as above in 25 mM Tris, pH 7.5, 150 mM NaCl, 25 mM imidazole, and 10% (v/v) glycerol. The cleared lysate was loaded on a 5-ml Nickel HP column (GE Healthcare), washed with the same buffer, and eluted with 25 mM Tris, pH 7.5, 150 mM NaCl, 500 mM imidazole, and 10% (v/v) glycerol. The protein was further purified by chromatography though a HiLoad 16/600 Superdex 200 column (GE Healthcare) in 25 mM Tris, pH 8.0, 300 mM NaCl, 10% (v/v) glycerol, 5 mM $MgCl_2$, 1 mM EDTA, and 2 mM DTT. The protein eluted from the gel filtration column at a purity ≥95% as judged by SDS-PAGE.

Constructs encoding biotinylated CBM for AlphaScreen assays were expressed in *E. coli* BL21(DE3) cells from a pETDuet (Novagen) derivative vector. The first T7 polymerase-driven expression unit of this vector contains the CBM ORF (human AMPK β1, residues 78–163, or β2, residues 76–163) as His_6-SUMO-avitag fusion, the second site the *E. coli* biotin-ligase gene *BirA*. The 14-amino acid avitag functions as a defined *in vivo* biotinylation site in *E. coli* (41). Cells grown in the presence of 40 μM biotin were lysed and fusion protein was purified over Nickel HiTrap columns as above. The His_6-SUMO tag was released by SUMO protease His_6-Ulp1 during overnight dialysis against 25 mM Tris, pH 7.5, 150 mM NaCl, 25 mM imidazole, and 10% (v/v) glycerol. Tags, uncleaved protein, and protease were removed by binding to a second Nickel HiTrap column. Biotin-Avitag-CBM proteins were further purified through a HiLoad 16/600 Superdex 200 column (GE Healthcare) in 25 mM Tris, pH 8.0, 300 mM NaCl, 10% (v/v) glycerol, 5 mM $MgCl_2$, 1 mM EDTA, and 2 mM DTT. The protein eluted from the gel filtration column at a purity ≥95% as judged by SDS-PAGE.

The volumes of the ADaM site ligand-binding pockets were calculated with the program Voidoo (42) using program default parameters and a probe with a radius of 1.4 Å. All structure figures were prepared using PyMOL (DeLano Scientific LLC, Palo Alto, CA).

Kinase assays

10 nM phosphorylated, or 1 μM nonphosphorylated, AMPK were incubated with 14 μM His_6-GST-SAMS in 10 mM Tris, pH 8.0, 5 mM $MgCl_2$, 150 mM NaCl, 1 mM EDTA, 2 mM DTT, 250 μM unlabeled ATP, and 2 μCi of [γ-^{32}P]ATP for 10–20 min at room temperature in a total volume of 15 μl. Reactions were terminated by boiling in SDS sample buffer and subjected to Tricine SDS-PAGE. Gels were stained with Coomassie Blue and destained with 10% (v/v) methanol, 10% (v/v) acetic acid, dried, and subjected to autoradiography using a FLA-5000 PhosphorImager (Fujifilm, Minato, Japan) and quantitated using ImageGauge software.

Phosphoprotein gel stain

SDS-PAGE gels were fixed by two rounds of incubation in ~100 ml of fix solution (50% methanol and 10% acetic acid) for 30 min at room temperature with gentle agitation. Gels were then washed three times in ~100 ml of ultrapure water with gentle agitation for 10 min, each, and stained by incubation in 60 ml of Pro-Q® Diamond phosphoprotein gel stain (Sigma) with gentle agitation in the dark for 60–90 min. Gels were destained three times for 40 min, each, in 100 ml of destain solution (20% acetonitrile, 50 mM sodium acetate, pH 4.0) with gentle agitation at room temperature, protected from light. Following destaining by two 4-min washes with ultrapure water at room temperature, gels were imaged using a Geliance 600 Imaging System (PerkinElmer Inc., Waltham, MA).

AlphaScreen assay

In vitro interactions between biotinylated CBM and His_6-tagged KD proteins were assessed by luminescence proximity AlphaScreen (PerkinElmer Life Sciences) technology. Briefly, the biotinylated binding partners were attached to streptavidin-coated donor beads, and His_6-tagged proteins were attached to nickel-chelated acceptor beads. The donor and acceptor beads were brought into proximity by the interactions between the His-tagged and biotinylated binding partners. When excited by a laser beam of 680 nm, the donor beads emit singlet oxygen that activates thioxene derivatives in the acceptor beads, which releases photons of 520–620 nm as the binding signal. The experiments were conducted at different stringency levels, with 100 nM CBM, 100 nM KD, and 0.1 mg/ml of bovine serum albumin (BSA; standard stringency) in Figs. 4 and 8*A*; 50 nM CBM, 100 nM KD, and no BSA (low stringency) in Fig. S6*A*; 50 nM CBM, 100 nM KD, and 0.2 mg/ml of BSA (moderate stringency) in Fig. S6*B*; and with ~25 nM bead-bound CMB, ~50 nM bead-bound KD, 0.2 mg/ml of BSA (high stringency) in Fig. S6*C* in the presence of 5 μg/ml of donor and acceptor beads, each, in a buffer of 50 mM MOPS, pH 7.4, 50 mM NaF, and 50 μM CHAPS. The results were based on three experiments (2 experiments for Fig. S6*C*) with standard errors typically less than 10% of the measurements.

Pulsed DEER spectroscopy

For pulsed DEER spectroscopy, a 20–35-μl sample of spin-labeled protein in a buffer solution containing 20% (v/v) glycerol was placed in a 2.0/2.4-mm borosilicate capillary (Vitrocom, Mountain Lakes, NJ) and then flash frozen in liquid nitrogen. Sample temperature was maintained at 50 K by a recirculating/closed-loop helium cryocooler and compressor system (Cold Edge Technologies, Allentown, PA). The four-pulse Q-band DEER experiments were conducted on a Bruker Elexsys 580 spectrometer fitted with a E5106400 cavity resonator. Pulse lengths were optimized via a nutation experiment but ranged from 12 to 22 ns ($\pi/2$) and 24 to 44 ns (π); pulses were amplified with a TWT amplifier (Applied Engineering Systems, Fort Worth, TX). Observed frequency was set to a spectral position 2 G downfield of the low and central resonance point of inflection, and the pump envelope was a 50-MHz wide square-chirp pulse (generated by a Bruker arbitrary waveform generator) set at 70 MHz down frequency from the observed position. All dipolar data were analyzed using a custom program ("Long Distances") written by Christian Altenbach in LabVIEW (National Instruments Corp., Austin, TX); software is available online (43) and its use is described elsewhere (44). All background-subtracted dipolar evolution data are shown in Figs. S7–S9. Peak uncertainty ranges (*gray* shaded area in all spectra) were obtained by minute perturbation of DEER analysis background subtraction function and by combining the resulting fits; this procedure is automated on the "errors" tab of "long distances."

Spin label modeling

Initial models of HO-225 spin-labeled 991-bound (PDB 4CFE) and cyclodextrin-bound (PDB 4RER) AMPK were generated by fixed backbone design "fixbb" within Rosetta3.6 using RosettaEPR's "R1A" side chain parameters (45, 46). Backbone restrained all-atom refinement was performed using Rosetta's standard "relax" protocol with increased $\chi1/\chi2$ rotamer sampling to generate 1000 possible structures for both HO-225 labeled AMPKs. The most energetically favorable model, as determined by the internal Rosetta energy function, was used for Fig. 1 and Fig. S5 and for calculation of label distances. Rosetta inputs and pipeline are available upon request.

Author contributions—X. G., M. D. B., Y. Y., X. E. Z., K. M. S.-P., W. L. H., and K. M. investigation; X. G., M. D. B., Y. Y., P. W. d. W., and W. L. H. methodology; X. G., M. D. B., Y. Y., P. W. d. W., X. E. Z., H. E. X., and W. L. H. writing-review and editing; M. D. B., H. E. X., W. L. H., and K. M. conceptualization; M. D. B., W. L. H., and K. M. data curation; M. D. B., K. M. S.-P., H. E. X., W. L. H., and K. M. formal analysis; M. D. B., W. L. H., and K. M. validation; M. D. B., P. W. d. W., and X. E. Z. visualization; H. E. X., W. L. H., and K. M. supervision; H. E. X., W. L. H., and K. M. funding acquisition; W. L. H. resources; W. L. H. and K. M. project administration; K. M. writing-original draft.

Acknowledgment—We thank Michelle Martin for administrative support.

References

1. Cheung, P. C., Salt, I. P., Davies, S. P., Hardie, D. G., and Carling, D. (2000) Characterization of AMP-activated protein kinase γ-subunit isoforms and their role in AMP binding. *Biochem. J.* **346,** 659–669 CrossRef Medline
2. Stapleton, D., Gao, G., Michell, B. J., Widmer, J., Mitchelhill, K., Teh, T., House, C. M., Witters, L. A., and Kemp, B. E. (1994) Mammalian 5′-AMP-activated protein kinase non-catalytic subunits are homologs of proteins that interact with yeast Snf1 protein kinase. *J. Biol. Chem.* **269,** 29343–29346 Medline
3. Thornton, C., Snowden, M. A., and Carling, D. (1998) Identification of a novel AMP-activated protein kinase β subunit isoform that is highly expressed in skeletal muscle. *J. Biol. Chem.* **273,** 12443–12450 CrossRef Medline
4. Gu, X., Yan, Y., Novick, S. J., Kovich, A., Goswami, D., Ke, J., Tan, M. H. E., Wang, L., Li, X., de Waal, P., Webb, M. R., Griffin, P. R., Xu, H. E., and Melcher, K. (2017) Deconvoluting AMP-dependent kinase (AMPK) adenine nucleotide binding and sensing. *J. Biol. Chem.* 292, 12653–12666 Medline
5. Xiao, B., Heath, R., Saiu, P., Leiper, F. C., Leone, P., Jing, C., Walker, P. A., Haire, L., Eccleston, J. F., Davis, C. T., Martin, S. R., Carling, D., and Gamblin, S. J. (2007) Structural basis for AMP binding to mammalian AMP-activated protein kinase. *Nature* **449,** 496–500 CrossRef Medline
6. Chen, L., Wang, J., Zhang, Y. Y., Yan, S. F., Neumann, D., Schlattner, U., Wang, Z. X., and Wu, J. W. (2012) AMP-activated protein kinase undergoes nucleotide-dependent conformational changes. *Nat. Struct. Mol. Biol.* **19,** 716–718 CrossRef Medline
7. Xiao, B., Sanders, M. J., Underwood, E., Heath, R., Mayer, F. V., Carmena, D., Jing, C., Walker, P. A., Eccleston, J. F., Haire, L. F., Saiu, P., Howell, S. A., Aasland, R., Martin, S. R., Carling, D., and Gamblin, S. J. (2011) Structure of mammalian AMPK and its regulation by ADP. *Nature* **472,** 230–233 CrossRef Medline
8. Hardie, D. G., Ross, F. A., and Hawley, S. A. (2012) AMPK: a nutrient and energy sensor that maintains energy homeostasis. *Nat. Rev. Mol. Cell Biol.* **13,** 251–262 CrossRef Medline
9. Hardie, D. G., Schaffer, B. E., and Brunet, A. (2016) AMPK: an energy-sensing pathway with multiple inputs and outputs. *Trends Cell Biol.* **26,** 190–201 CrossRef Medline
10. Steinberg, G. R., and Kemp, B. E. (2009) AMPK in health and disease. *Physiol. Rev.* **89,** 1025–1078 CrossRef Medline
11. Langendorf, C. G., and Kemp, B. E. (2015) Choreography of AMPK activation. *Cell Res.* **25,** 5–6 CrossRef Medline
12. Polekhina, G., Gupta, A., Michell, B. J., van Denderen, B., Murthy, S., Feil, S. C., Jennings, I. G., Campbell, D. J., Witters, L. A., Parker, M. W., Kemp, B. E., and Stapleton, D. (2003) AMPK β subunit targets metabolic stress sensing to glycogen. *Curr. Biol.* **13,** 867–871 CrossRef Medline
13. Li, X., Wang, L., Zhou, X. E., Ke, J., de Waal, P. W., Gu, X., Tan, M. H., Wang, D., Wu, D., Xu, H. E., and Melcher, K. (2015) Structural basis of AMPK regulation by adenine nucleotides and glycogen. *Cell Res.* **25,** 50–66 CrossRef Medline
14. McBride, A., Ghilagaber, S., Nikolaev, A., and Hardie, D. G. (2009) The glycogen-binding domain on the AMPK β subunit allows the kinase to act as a glycogen sensor. *Cell Metab.* **9,** 23–34 CrossRef Medline
15. Calabrese, M. F., Rajamohan, F., Harris, M. S., Caspers, N. L., Magyar, R., Withka, J. M., Wang, H., Borzilleri, K. A., Sahasrabudhe, P. V., Hoth, L. R., Geoghegan, K. F., Han, S., Brown, J., Subashi, T. A., Reyes, A. R., *et al.* (2014) Structural basis for AMPK activation: natural and synthetic ligands regulate kinase activity from opposite poles by different molecular mechanisms. *Structure* **22,** 1161–1172 CrossRef Medline
16. Xiao, B., Sanders, M. J., Carmena, D., Bright, N. J., Haire, L. F., Underwood, E., Patel, B. R., Heath, R. B., Walker, P. A., Hallen, S., Giordanetto, F., Martin, S. R., Carling, D., and Gamblin, S. J. (2013) Structural basis of AMPK regulation by small molecule activators. *Nat. Commun.* **4,** 3017 CrossRef Medline
17. Göransson, O., McBride, A., Hawley, S. A., Ross, F. A., Shpiro, N., Foretz, M., Viollet, B., Hardie, D. G., and Sakamoto, K. (2007) Mechanism of action of A-769662, a valuable tool for activation of AMP-activated protein kinase. *J. Biol. Chem.* **282,** 32549–32560 CrossRef Medline
18. Sanders, M. J., Ali, Z. S., Hegarty, B. D., Heath, R., Snowden, M. A., and Carling, D. (2007) Defining the mechanism of activation of AMP-activated protein kinase by the small molecule A-769662, a member of the thienopyridone family. *J. Biol. Chem.* **282,** 32539–32548 CrossRef Medline
19. Gowans, G. J., Hawley, S. A., Ross, F. A., and Hardie, D. G. (2013) AMP is a true physiological regulator of AMP-activated protein kinase by both allosteric activation and enhancing net phosphorylation. *Cell Metab.* **18,** 556–566 CrossRef Medline
20. Oakhill, J. S., Steel, R., Chen, Z. P., Scott, J. W., Ling, N., Tam, S., and Kemp, B. E. (2011) AMPK is a direct adenylate charge-regulated protein kinase. *Science* **332,** 1433–1435 CrossRef Medline
21. Hardie, D. G. (2017) Targeting an energy sensor to treat diabetes. *Science* **357,** 455–456 CrossRef Medline
22. Hardie, D. G. (2013) AMPK: a target for drugs and natural products with effects on both diabetes and cancer. *Diabetes* **62,** 2164–2172 CrossRef Medline
23. Cokorinos, E. C., Delmore, J., Reyes, A. R., Albuquerque, B., Kjobsted, R., Jørgensen, N. O., Tran, J. L., Jatkar, A., Cialdea, K., Esquejo, R. M., Meissen, J., Calabrese, M. F., Cordes, J., Moccia, R., Tess, D., *et al.* (2017) Activation of skeletal muscle AMPK promotes glucose disposal and glucose lowering in non-human primates and mice. *Cell Metab.* **25,** 1147–1159.e10 CrossRef Medline
24. Myers, R. W., Guan, H. P., Ehrhart, J., Petrov, A., Prahalada, S., Tozzo, E., Yang, X., Kurtz, M. M., Trujillo, M., Gonzalez Trotter, D., Feng, D., Xu, S., Eiermann, G., Holahan, M. A., Rubins, D., *et al.* (2017) Systemic pan-AMPK activator MK-8722 improves glucose homeostasis but induces cardiac hypertrophy. *Science* **357,** 507–511 CrossRef Medline
25. Wu, J., Puppala, D., Feng, X., Monetti, M., Lapworth, A. L., and Geoghegan, K. F. (2013) Chemoproteomic analysis of intertissue and interspecies isoform diversity of AMP-activated protein kinase (AMPK). *J. Biol. Chem.* **288,** 35904–35912 CrossRef Medline
26. Ngoei, K. R. W., Langendorf, C. G., Ling, N. X. Y., Hoque, A., Johnson, S., Camerino, M. C., Walker, S. R., Bozikis, Y. E., Dite, T. A., Ovens, A. J., Smiles, W. J., Jacobs, R., Huang, H., Parker, M. W., *et al.* (2018) Structural determinants for small-molecule activation of skeletal muscle AMPK α2β2γ1 by the glucose importagog SC4. *Cell Chem. Biol.* **25,** 728–737 Medline
27. Scott, J. W., van Denderen, B. J., Jorgensen, S. B., Honeyman, J. E., Steinberg, G. R., Oakhill, J. S., Iseli, T. J., Koay, A., Gooley, P. R., Stapleton, D., and Kemp, B. E. (2008) Thienopyridone drugs are selective activators of AMP-activated protein kinase β1-containing complexes. *Chem. Biol.* **15,** 1220–1230 CrossRef Medline
28. Scott, J. W., Ling, N., Issa, S. M., Dite, T. A., O'Brien, M. T., Chen, Z. P., Galic, S., Langendorf, C. G., Steinberg, G. R., Kemp, B. E., and Oakhill, J. S. (2014) Small molecule drug A-769662 and AMP synergistically activate naive AMPK independent of upstream kinase signaling. *Chem. Biol.* **21,** 619–627 CrossRef Medline
29. Willows, R., Sanders, M. J., Xiao, B., Patel, B. R., Martin, S. R., Read, J., Wilson, J. R., Hubbard, J., Gamblin, S. J., and Carling, D. (2017) Phosphorylation of AMPK by upstream kinases is required for activity in mammalian cells. *Biochem. J.* **474,** 3059–3073 CrossRef Medline
30. Scott, J. W., Galic, S., Graham, K. L., Foitzik, R., Ling, N. X., Dite, T. A., Issa, S. M., Langendorf, C. G., Weng, Q. P., Thomas, H. E., Kay, T. W., Birnberg, N. C., Steinberg, G. R., Kemp, B. E., and Oakhill, J. S. (2015) Inhibition of AMP-activated protein kinase at the allosteric drug-binding site promotes islet insulin release. *Chem. Biol.* **22,** 705–711 CrossRef Medline
31. Altenbach, C., Kusnetzow, A. K., Ernst, O. P., Hofmann, K. P., and Hubbell, W. L. (2008) High-resolution distance mapping in rhodopsin reveals the pattern of helix movement due to activation. *Proc. Natl. Acad. Sci. U.S.A.* **105,** 7439–7444 CrossRef
32. Jeschke, G. (2012) DEER distance measurements on proteins. *Annu. Rev. Phys. Chem.* **63,** 419–446 CrossRef Medline
33. Pannier, M., Veit, S., Godt, A., Jeschke, G., and Spiess, H. W. (2000) Dead-time free measurement of dipole-dipole interactions between electron spins. *J. Magn. Reson.* **142,** 331–340 CrossRef Medline

34. Shao, D., Oka, S., Liu, T., Zhai, P., Ago, T., Sciarretta, S., Li, H., and Sadoshima, J. (2014) A redox-dependent mechanism for regulation of AMPK activation by thioredoxin1 during energy starvation. *Cell Metab.* **19,** 232–245 CrossRef Medline
35. Willows, R., Navaratnam, N., Lima, A., Read, J., and Carling, D. (2017) Effect of different γ-subunit isoforms on the regulation of AMPK. *Biochem. J.* **474,** 1741–1754 CrossRef Medline
36. Kornev, A. P., Haste, N. M., Taylor, S. S., and Eyck, L. F. (2006) Surface comparison of active and inactive protein kinases identifies a conserved activation mechanism. *Proc. Natl. Acad. Sci. U.S.A.* **103,** 17783–17788 CrossRef Medline
37. Jin, L., Pluskey, S., Petrella, E. C., Cantin, S. M., Gorga, J. C., Rynkiewicz, M. J., Pandey, P., Strickler, J. E., Babine, R. E., Weaver, D. T., and Seidl, K. J. (2004) The three-dimensional structure of the ZAP-70 kinase domain in complex with staurosporine: implications for the design of selective inhibitors. *J. Biol. Chem.* **279,** 42818–42825 CrossRef Medline
38. Polekhina, G., Gupta, A., van Denderen, B. J., Feil, S. C., Kemp, B. E., Stapleton, D., and Parker, M. W. (2005) Structural basis for glycogen recognition by AMP-activated protein kinase. *Structure* **13,** 1453–1462 CrossRef Medline
39. Oligschlaeger, Y., Miglianico, M., Chanda, D., Scholz, R., Thali, R. F., Tuerk, R., Stapleton, D. I., Gooley, P. R., and Neumann, D. (2015) The recruitment of AMP-activated protein kinase to glycogen is regulated by autophosphorylation. *J. Biol. Chem.* **290,** 11715–11728 CrossRef Medline
40. Kornev, A. P., and Taylor, S. S. (2015) Dynamics-driven allostery in protein kinases. *Trends Biochem. Sci.* **40,** 628–647 CrossRef Medline
41. Smith, P. A., Tripp, B. C., DiBlasio-Smith, E. A., Lu, Z., LaVallie, E. R., and McCoy, J. M. (1998) A plasmid expression system for quantitative *in vivo* biotinylation of thioredoxin fusion proteins in *Escherichia coli*. *Nucleic Acids Res.* **26,** 1414–1420 CrossRef Medline
42. Kleywegt, G. J., and Jones, T. A. (1994) Detection, delineation, measurement and display of cavities in macromolecular structures. *Acta Crystallogr. D Biol. Crystallogr.* **50,** 178–185 CrossRef Medline
43. Altenbach, C. (2017) *LongDistances,* version 593, LabVIEW National Instruments Corp., Austin, TX
44. Fleissner, M. R., Brustad, E. M., Kalai, T., Altenbach, C., Cascio, D., Peters, F. B., Hideg, K., Peuker, S., Schultz, P. G., and Hubbell, W. L. (2009) Site-directed spin labeling of a genetically encoded unnatural amino acid. *Proc. Natl. Acad. Sci. U.S.A.* **106,** 21637–21642 CrossRef
45. Alexander, N. S., Stein, R. A., Koteiche, H. A., Kaufmann, K. W., McHaourab, H. S., and Meiler, J. (2013) RosettaEPR: rotamer library for spin label structure and dynamics. *PLoS ONE* **8,** e72851 CrossRef Medline
46. Leaver-Fay, A., Tyka, M., Lewis, S. M., Lange, O. F., Thompson, J., Jacak, R., Kaufman, K., Renfrew, P. D., Smith, C. A., Sheffler, W., Davis, I. W., Cooper, S., Treuille, A., Mandell, D. J., Richter, F., *et al.* (2011) ROSETTA3: an object-oriented software suite for the simulation and design of macromolecules. *Methods Enzymol.* **487,** 545–574 CrossRef Medline